Local structure of the metal-organic perovskite dimethylammonium manganese(II) formate

H. D. Duncan, M. T. Dove, D. A. Keen, and A. E. Phillips

Electronic Supplementary Information

Contents

1 Data collection run numbers

The raw data from this experiment are stored in the ISIS archive, experiment number 1210310, available at `https://data.isis.stfc.ac.uk`, with run numbers given in Table S1.

For the nominal 190 K measurement, the measured sample temperature is close to that of the phase transition at 183 K. Nonetheless the Bragg profile for the 190K sample shows no peak at d-spacing 6.90 Å, which would be expected if the low-temperature phase were accidentally present.

Table S1: Collection run numbers for long data sets $> 150\,\mu\text{A h}$ for DMMnF, values in brackets are maximum ranges, i.e. 243.1(6)K is 243.1 ± 0.3 K. *range for run GEM60024 = 247 K to 242.6 K

$T_{\text{nominal}}/\text{K}$	T_{CCR}/K	$T_{\text{sample}}/\text{K}$	Run numbers	Total proton beam charge /$\mu\text{A h}$
293	–	300.9(5)	GEM60010–GEM60018	1288
250	250	243.1(6)*	GEM60024–GEM60031	1200
225	225	218.3(1)	GEM60133–GEM60136	508
200	200	194.2(1)	GEM60037–GEM60044	1200
190	190	184.5(5)	GEM60050	150
180	180	175.0(5)	GEM60056	150
170	170	165.5(5)	GEM60062	150
160	160	155.4(3)	GEM60068	150
150	150	145.6(1)	GEM60074–GEM60081	1200
100	100	97.4(1)	GEM60087–GEM60094	1200
20	20.2(1)	21.5(1)	GEM60100–GEM60106	1050
7	4.75(3)	6.81(3)	GEM60117–GEM60122	900

The run numbers for background and normalisation measurements are given in Table S2.

Table S2: Run numbers required for normalisation and background corrections

Description	Run number	Description	Total proton beam charge /$\mu\text{A h}$
Normalisation	GEM60002	8mm V rod	500
Normalisation background	GEM60003	Empty GEM	150
Sample background	GEM60004	Empty CCR	200
Container	GEM60005–GEM60008	Empty vanadium can	600

2 Restraints applied to refinements

The restraints applied during Rietveld and RMC refinements are listed in tables S3, S4, and S5 below:

Table S3: Bond types and restraints applied to them during GSAS refinement.

Bond type	Restraint length /Å
C–D (DMA)	1.050
C–D (formate)	1.050
N–D	1.050
Mn–O	2.180
C≡O (formate)[*]	1.250

[*] applied to the low-temperature phase only

Table S4: Morse bond stretch potentials used to constrain RMC refinement, according to the penalty term $E = D(1 - \exp\{-\alpha(r - r_0)\})^2$. We set $\alpha = 2.55\,\text{Å}^{-1}$ throughout, in accordance with the MM3 potential set.

Atomic pair	D/eV	$r_0/\text{Å}$
C–N	2.051	1.50
C≡O	3.376	1.24
C–D	2.275	1.06
N–D	2.947	1.06

Table S5: Angle potentials used to constrain RMC refinement, according to the penalty term $E = \frac{1}{2}k(\cos\theta - \cos\theta_0)^2$.

Atoms	k/eV	$\theta_0/^\circ$
O≡C≡O	17.876	129.800
C–N–C	7.864	108.600
D–C–D	8.976	107.114
C–N–D	7.602	106.376
D–C–O	7.403	114.900
N–C–D	11.235	104.700
C–N–D	6.504	105.949

Table S6: Distance windows applied to RMC refinements

T/K	D–C	D–N	C–O	C–N	O–Mn
293	0.9091 - 1.1288	0.9482 - 1.1726	1.1179 - 1.3783	1.3311 - 1.6420	2.0751 - 2.3625
250	0.9207 - 1.1403	0.9484 - 1.1732	1.1161 - 1.3761	1.3261 - 1.6361	2.0713 - 2.3582
200	0.9478 - 1.1713	0.9485 - 1.1736	1.1152 - 1.3750	1.3229 - 1.6326	2.0693 - 2.3560
150	0.9229 - 1.2262	0.9310 - 1.2100	1.1431 - 1.3483	1.3657 - 1.7030	2.0156 - 2.3755
100	0.9268 - 1.2436	0.9300 - 1.2174	1.1632 - 1.3570	1.3606 - 1.7179	2.0206 - 2.3184
20	0.9290 - 1.2640	0.9338 - 1.2340	1.1638 - 1.3642	1.3682 - 1.7350	2.0312 - 2.3154
7	0.9257 - 1.2446	0.9272 - 1.2256	1.1637 - 1.3762	1.3677 - 1.7227	1.9984 - 2.3529

3 Lattice parameters

The lattice parameters for the high and low temperature phases obtained from Rietveld refinement, expressed in terms of the monoclinic Cc cell, are given in Table S7 below:

Table S7: Lattice parameters in terms of the Cc cell

| $T_{\text{nominal}}/\text{K}$	$T_{\text{sample}}/\text{K}$	$a/\text{Å}$	$b/\text{Å}$	$c/\text{Å}$	$\beta/°$
293	300.9(5)	14.4347(4)	8.3339(2)	9.0141(3)	122.261(9)
250	243.1(6)	14.4314(4)	8.3332(2)	8.8907(3)	122.388(9)
225	218.3(1)	14.4351(4)	8.3341(2)	8.9722(3)	122.431(9)
200	194.2(1)	14.4316(4)	8.3321(2)	8.9612(3)	122.467(9)
190	184.5(5)	14.4340(4)	8.3335(2)	8.9602(3)	122.478(9)
180	175.0(5)	14.3746(3)	8.3208(2)	8.8852(2)	120.831(1)
170	165.5(5)	14.3707(3)	8.3207(2)	8.8815(2)	120.810(1)
160	155.4(3)	14.3675(3)	8.3209(2)	8.8778(2)	120.798(1)
150	145.6(1)	14.3628(3)	8.3214(2)	8.8734(1)	120.784(1)
100	97.4(1)	14.3530(3)	8.3214(2)	8.8582(2)	120.781(1)
20	21.5(1)	14.3477(3)	8.3231(2)	8.8454(2)	120.802(1)
7	6.81(3)	14.3460(4)	8.3222(2)	8.8446(2)	120.799(2)

The lattice parameters for the high temperature phase obtained from Rietveld refinement, expressed in terms of the original $R\bar{3}c$ cell, are given in Table S8 below:

Table S8: Lattice parameters in terms of the $R\bar{3}c$ cell where $a = b$ and $\alpha = \beta = 90°, \gamma = 120°$

| $T_{\text{nominal}}/\text{K}$	$T_{\text{sample}}/\text{K}$	$a/\text{Å}$	$c/\text{Å}$
293	300.9(5)	8.3340(3)	22.868(1)
250	243(3)	8.3320(3)	22.751(1)
225	218.3(1)	8.3341(3)	22.718(1)
200	194.2(1)	8.3321(3)	22.682(1)
190	184.5(5)	8.3335(3)	22.676(1)

4 Convergence criteria

Representative convergence plots for the three data sets models were refined against are given in Figure S1 below. RMC was run for four days for each configuration, corresponding to approximately 1.5×10^7 atomic moves in the high-temperature phase and 1.8×10^7 atomic moves in the low-temperature phase.
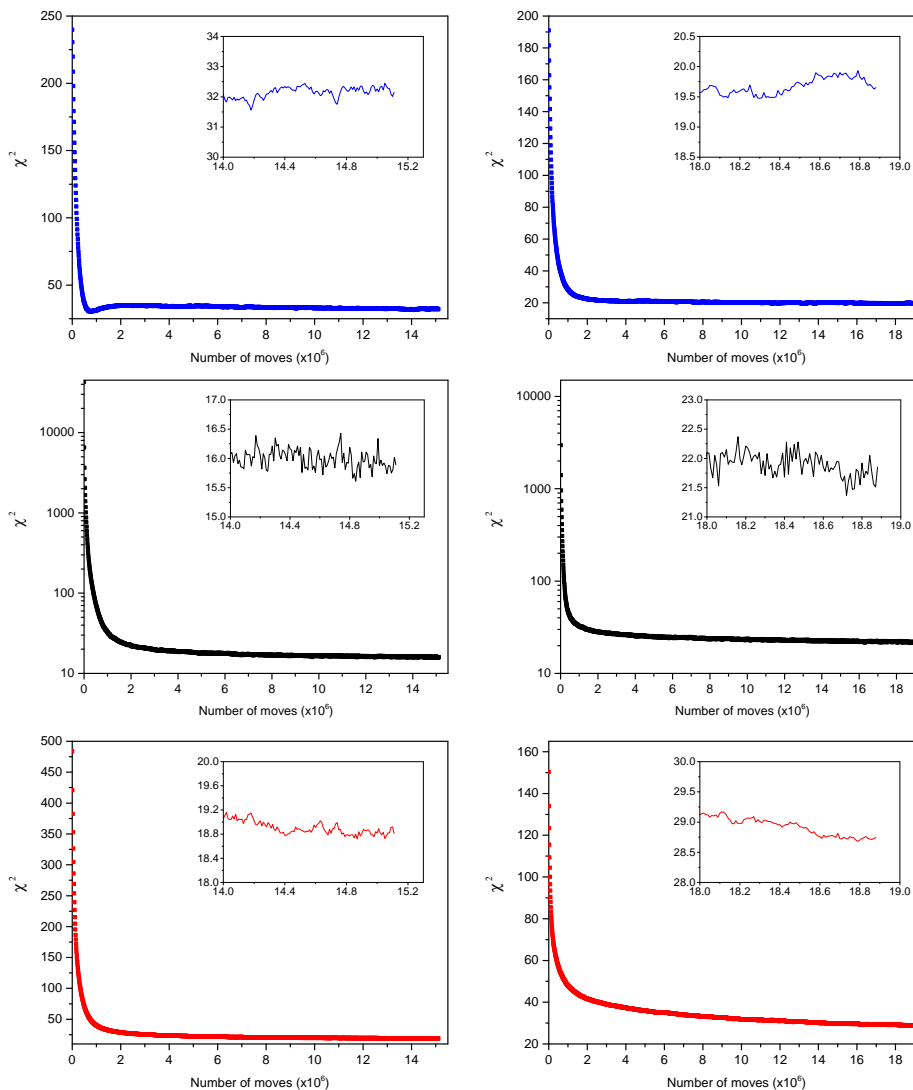
Figure S1: Representative χ^2 plotted as a function of the number of atomic moves made for the Bragg $I(t)$ (top), PDF $D(r)$ (middle), and scattering function $F(Q)$ (bottom) fits to $298\,\text{K}$ (left) and $150\,\text{K}$ (right) data.

5 Sample configurations

Representative initial configurations of DMMnF in both phases are shown in Figure S2 below:
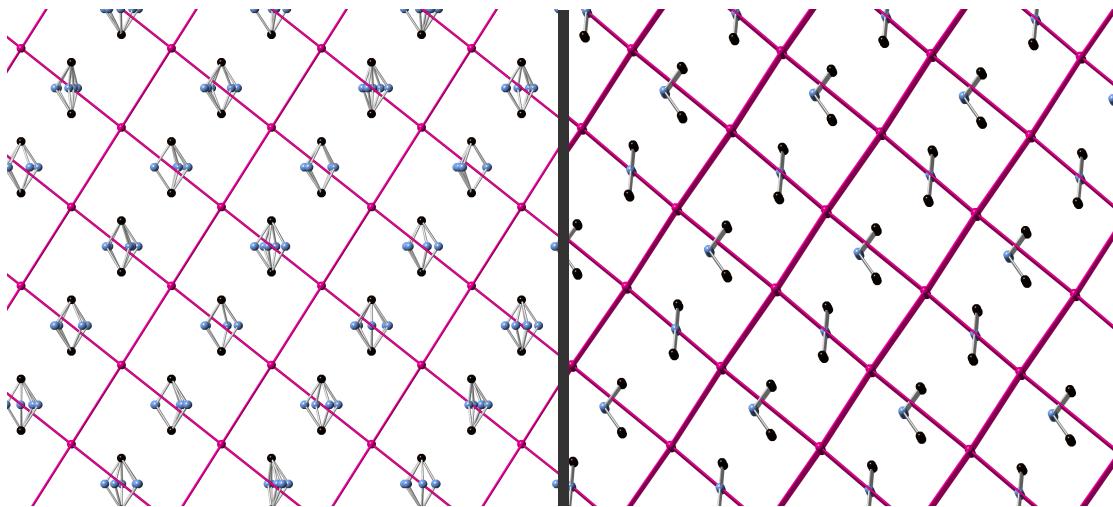
Figure S2: The initial configurations for a high (left) and low temperature (right) refinement with the $Mn(HCO_2)_3$ framework is displayed as pink lines, and the deuterium atoms omitted for clarity. In the high temperature configuration (model **1**), the ND_2 groups (blue nitrogen shown) are rotated randomly about the C$\cdots$C axis. In the low temperature phase the DMA cations are not rotated from their crystal structure.

6 Partial pair distribution functions

The partial pair distribution functions, averaged over 30 refined configurations starting from configuration **1**, for bonding pairs are given in Figure S3 below. All bonds appear physically reasonable apart from $Mn-O$, in which both sides of the peak are sharper than expected. This is due to the distance window applied to prevent $Mn-O$ pairs from moving outside an allowed range of separations. Increasing the size of the allowed window results in the $Mn-O$ pair density expanding to fill the new window so that the new peak edges remain unphysically sharp. This implies that the data are comparatively unsensitive to the exact length of this bond. Indeed, considering the neutron scattering lengths of the relevant nuclei (see main text) shows that the $Mn-O$ peak in the PDF is of only moderate intensity and negative; moreover, it is in the same region as several strong positive peaks, in particular intramolecular $D{\cdots}N$ and $D{\cdots}C$ distances from the DMA ion.

The distance windows for our final analysis were chosen to allow reasonable distances either side of the Rietveld refined values. The exact distance window values, though, did not affect our conclusions.
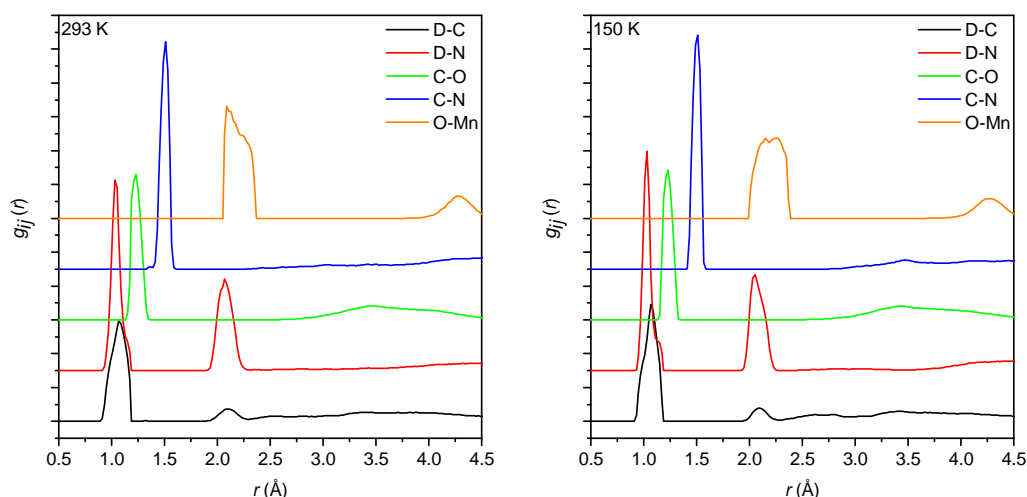

Figure S3: Partial PDFs for bonding pairs averaged over 30 individual configurations at $293\,K$ (left) and $150\,K$ (right).

In figures S4 and S5 below, we compare the residual PDF $D_{exp}(r) - D_{model}(r)$ to the partial PDFs over the crucial region between $2\,\text{Å}$ and $3.5\,\text{Å}$. In particular, the residual is greater than $g_{NO}(r)$ in the high-temperature phase, but less in the low-temperature phase. This should not be taken, however, to mean that the distribution of $N{\cdots}O$ distances cannot be determined in the high-temperature phase: see discussion in main text.
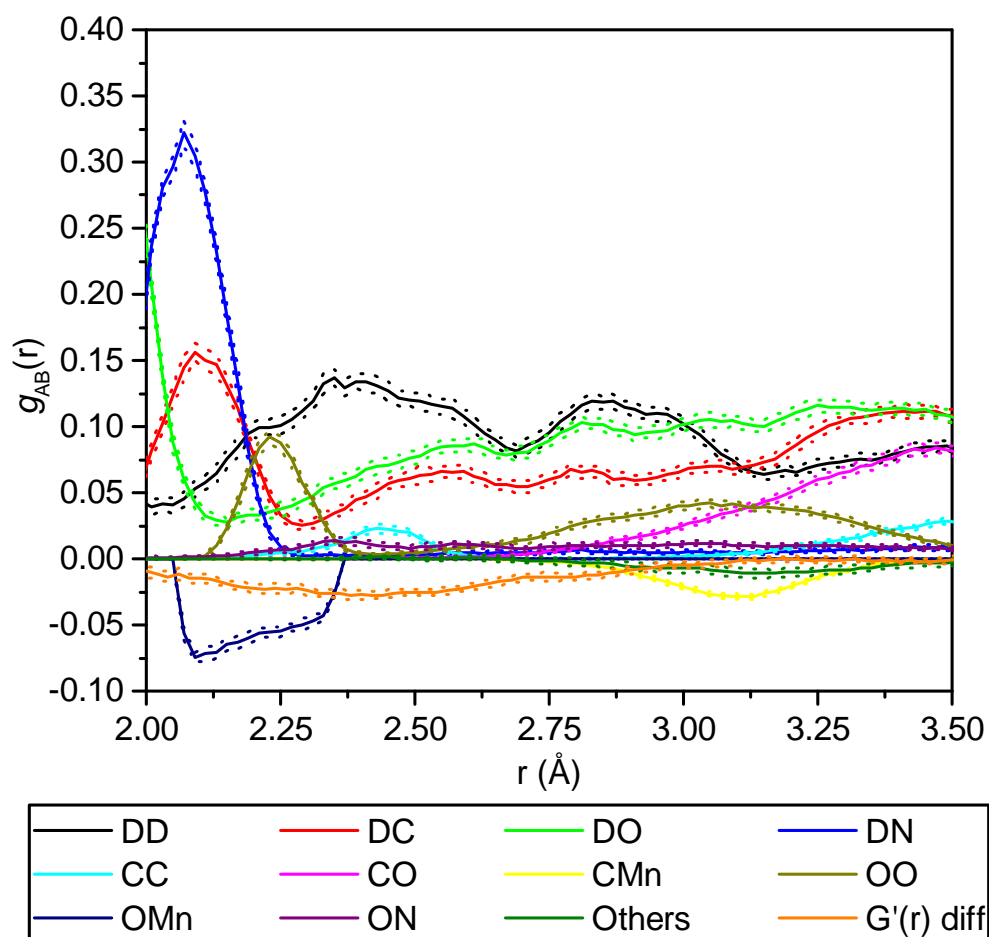
Figure S4: Scaled partial pair distribution functions contributing significantly to $D(r)$ between $2\,\text{Å}$ and $3.5\,\text{Å}$, along with the residual between the experimental and modelled PDF. All partial PDFs not explicitly shown are summed as "Others". Dotted lines show $\pm\sigma$ from 30 runs refining model **1** against the $293\,\text{K}$ data.
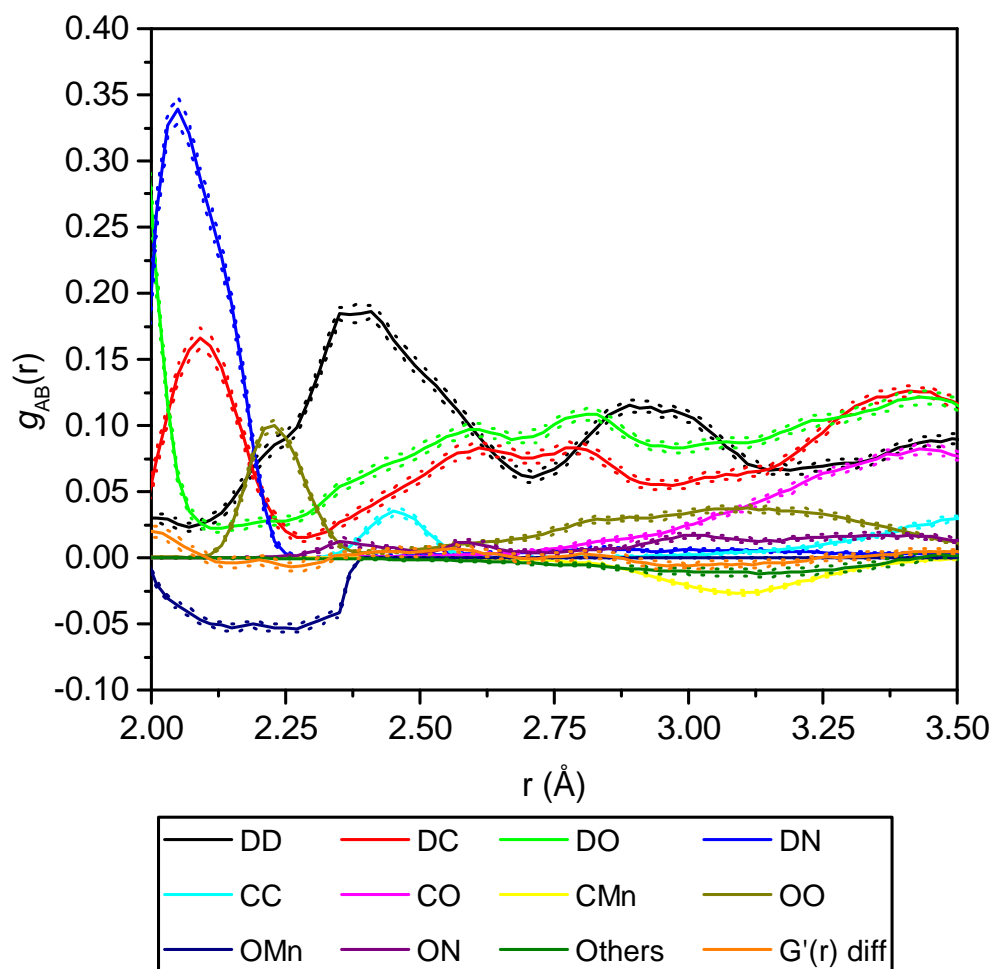
Figure S5: Scaled partial pair distribution functions contributing significantly to $D(r)$ between $2\,\text{Å}$ and $3.5\,\text{Å}$, along with the residual between the experimental and modelled PDF. All partial PDFs not explicitly shown are summed as "Others". Dotted lines show $\pm\sigma$ from 30 runs refining against the $150\,\text{K}$ data.

7 Progress of refinements

Figure S6 below shows the evolution of the fits to the experimental data over the first twelve hours of refinement.
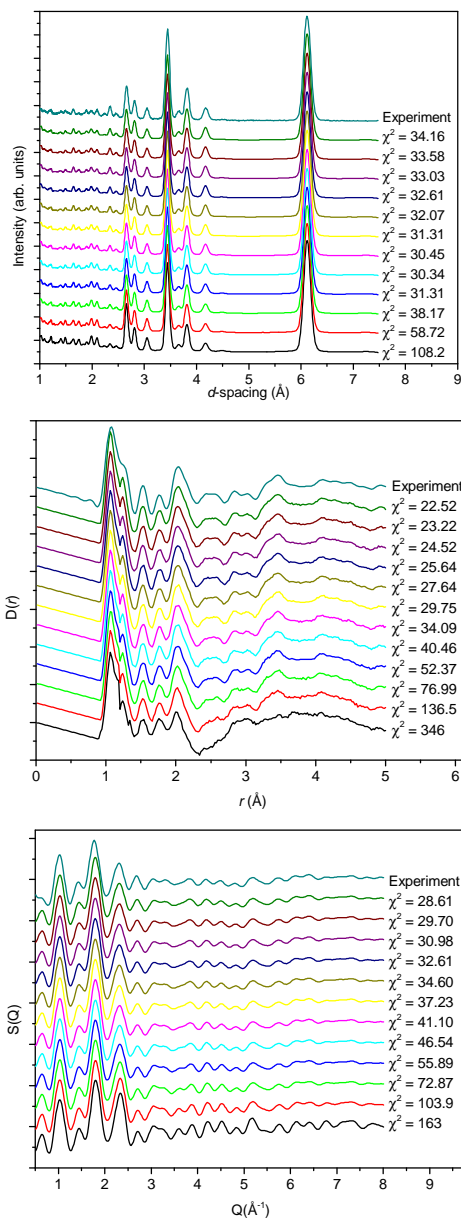
Figure S6: Evolution of the fits to the experimental data. Data (reading from bottom to top) were extracted each hour.

8 Representative fits

Representative fits to the $D(r)$, $I(t)$, and $F(Q)$ functions for the high-temperature phase are shown in Figure 6 of the main paper; the corresponding figure for the low-temperature phase is shown in Figure S7 below:
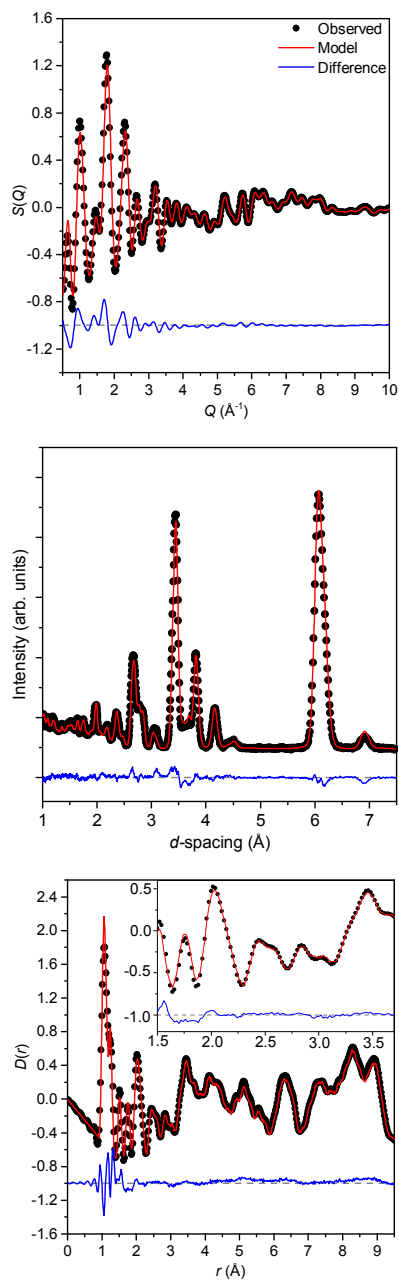
Figure S7: Experimental and fit functions $D(r)$, $S(Q)$, and $I(t)$ for a 150 K model

9 O–Mn–O bond angles

We report in the main text of the paper that on RMC refinement the $O-Mn-O$ bond angles in both phases merely broaden slightly from their average values. This is shown in figure S8 below:
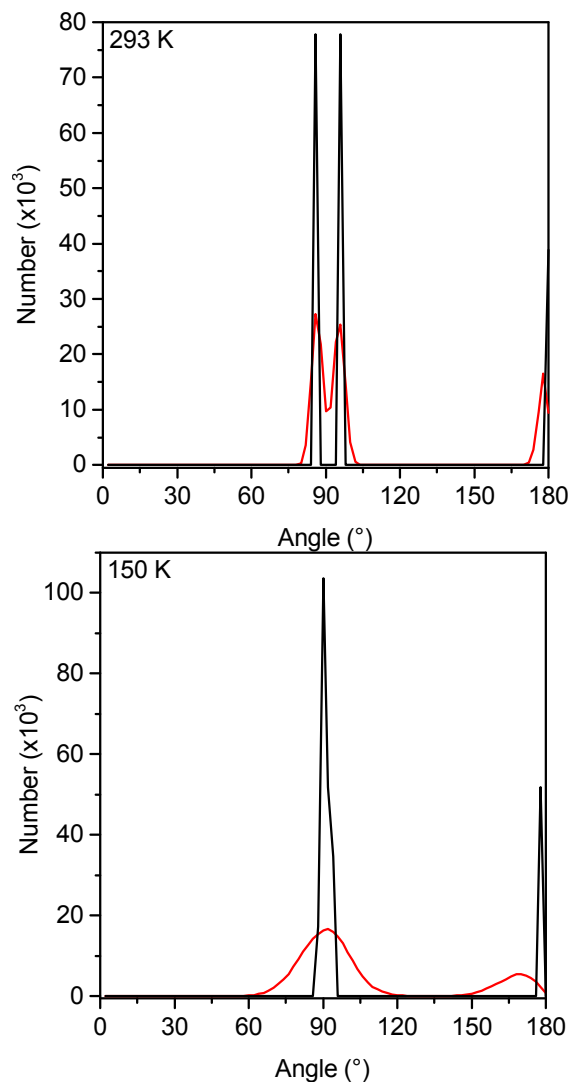
Figure S8: The initial (black) and final (red) distributions of the O–Mn–O angles of the MnO_6 octahedra at $293\,K$ (top) and $150\,K$ (bottom).